

Radiation Efficiency and Gain Bounds for Microstrip Patch Antennas

Ben A. P. Nel[✉], Anja K. Skrivelvik[✉], and Mats Gustafsson[✉], *Senior Member, IEEE*

Abstract—This article presents bounds on radiation efficiency and gain for microstrip patch antennas, demonstrating close alignment with the performance of classic antenna designs. These bounds serve as effective benchmarks for assessing antenna performance and evaluating trade-offs and design feasibility. The study particularly addresses the trade-off between miniaturization and performance by comparing bounds for antennas of similar size and frequency, achieved either by using high-permittivity substrates or by optimizing the metallic patch design area. To enhance usability, scaling laws are applied, enabling these bounds to be approximated across a range of frequencies using only data from a half-wavelength patch antenna simulation or measurement. Additionally, the study finds a strong correlation between the established radiation efficiency bounds and lower Q-factor limits (indicative of maximum bandwidth). This relationship is highly advantageous in the design process, as it illustrates how bandwidth and radiation efficiency can be optimized together.

Index Terms—Gain, method of moments (MoM), microstrip patch antennas, physical bounds, radiation efficiency.

I. INTRODUCTION

MICROSTRIP patch antennas have been widely used for several decades [1], [2], [3]. Today, these antennas can be accurately modeled using commercially available computational electromagnetic software, such as, FEKO [4] or CST [5]. Making use of these simulation tools, antenna designers are able to determine performance parameters including radiation efficiency, gain, and bandwidth.

Radiation efficiency and gain are crucial performance metrics for accessing antenna losses. However, there is limited knowledge about the performance limitations of these parameters in the context of microstrip patch antennas. Understanding these performance limitations can enhance the antenna design process and lead to innovative designs. Early work computing radiation efficiency and gain bounds for antennas in free space

Received 29 February 2024; revised 4 November 2024; accepted 26 November 2024. Date of publication 16 December 2024; date of current version 5 February 2025. This work was supported in part by the Excellence Center at Linköping-Lund in Information Technology (ELLIT) and in part by the Hedda Andersson Guest Professor Program at Lund University. (*Corresponding author: Ben A. P. Nel*)

Ben A. P. Nel and Mats Gustafsson are with the Department of Electrical and Information Technology, Lund University, 221 00 Lund, Sweden (e-mail: ben.nel@eit.lth.se; mats.gustafsson@eit.lth.se).

Anja K. Skrivelvik is with the Microwave Antenna Group, École Polytechnique Fédérale de Lausanne (EPFL), 1015 Lausanne, Switzerland, and also with the Department of Electrical and Information Technology, Lund University, 221 00 Lund, Sweden (e-mail: anja.skrivelvik@epfl.ch).

Digital Object Identifier 10.1109/TAP.2024.3514318

can be found in [6]. More recent work has focused on using current optimization to obtain radiation efficiency bounds for arbitrary geometries [7], [8].

The goal of this article is to aid microstrip patch antenna design by providing radiation efficiency and gain bounds. This is achieved by considering all possible patch geometries within a given design region using current optimization [9]. Some classical patch antenna designs are shown to perform near the bounds both for Ohmic losses in the patch region as well as for dielectric losses in the substrate. Therefore, practical design information is provided regarding the feasibility of obtaining the desired radiation efficiency as well as a benchmark to assess potential design improvements. The work presented here builds on previous formulations determining lower Q-factor bounds for microstrip patch antennas [10], [11].

In this article, a single-layer microstrip patch antenna is considered, where currents are confined horizontally within the patch design region. To reduce the computational complexity, the ground plane and dielectric substrate are assumed to be infinite. These assumptions are known to be reasonable for moderately sized ground planes and dielectric substrates [2]. These microstrip patch antennas can be fed, e.g., with a probe feed coming from the ground plane. Note that there exist methods that may be used to improve the radiation efficiency of a self-resonant microstrip patch antenna, for instance using a shorting pin or by reducing the size of the ground plane and dielectric substrate [12], [13], [14], [15], which are not considered here. However, the bounds presented here serve as a first canonical case for analyzing maximum radiation efficiency for antennas that are in wide use.

Here, miniaturization refers to reducing the patch design region below its natural resonance in free space, such as approximately half a free-space wavelength for a rectangular design. Two methods for achieving miniaturization are evaluated: increasing the substrate permittivity (which enlarges the electrical size of the design region) and shaping the patch by removing metal from the patch design region. The latter method can reduce the natural half wavelength (in the dielectric substrate) resonance frequency of the metal design region by forcing the current density around slots. Miniaturization is often required even though it is well known that reducing antenna size is challenging, coming at the cost of radiation efficiency [12], [13], [16].

Radiation efficiency and gain are recognized as critical design parameters for microstrip patch antennas, yet bandwidth is equally important for comprehensive performance

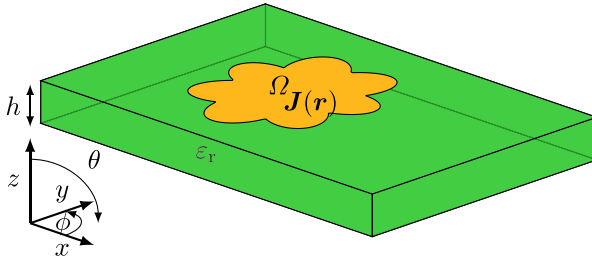


Fig. 1. Microstrip patch antenna design region is given by Ω . All metal patch geometries fitting within this region are considered. Surface current densities on this design region are denoted, $J(r)$. The infinite dielectric substrate with relative permittivity, ϵ_r , and thickness, h , is on top of an infinite PEC ground plane.

evaluation [10]. This article bridges the gap between maximum radiation efficiency and lower Q-factor bounds (directly related to the bandwidth). This is achieved by deriving an approximate expression that calculates radiation efficiency from the Q-factor. This relationship not only enhances the understanding of microstrip patch antenna performance but also provides a practical tool for antenna designers to optimize designs, ensuring that radiation efficiency and bandwidth are simultaneously addressed.

The remainder of the article is structured as follows. Section II introduces the microstrip patch antenna model and outlines the evaluation process for radiation efficiency and gain. Section III formulates the procedure to compute radiation efficiency and gain bounds using current optimization. Further, patch miniaturization is investigated in Section IV. Then, using derived semi-analytic expressions, Section V discusses bounds scaling for Ohmic and dielectric losses. Section VI provides a link between minimum Q-factor and maximum radiation efficiency. A brief discussion on adding vertical currents between the ground plane and patch antenna is presented in Section VII. The article is concluded in Section VIII. Finally, the appendices provide additional mathematical and procedural details and summarize the used variables.

II. MICROSTRIP PATCH ANTENNA MODEL

The geometry considered to model microstrip patch antennas is shown in Fig. 1, where the design region Ω , that can be of arbitrary shape, is situated at the interface between free space and a transversely infinite dielectric substrate. This dielectric, with relative permittivity ϵ_r and thickness h , is on top of an infinite PEC ground plane.

In this article, a rectangular design region, Ω , is chosen for simplicity; see Fig. 2(a). Classical patch geometries fitting within this rectangular design region, such as a half-wavelength patch (a) as well as miniaturized geometries that reduce the resonant frequency, e.g., slot loaded patch [17] (b), and H-shaped patch [17] (c), are shown in Fig. 2. The radiation efficiency and gain of these classical patch geometries serve as a reference with which to compare the presented bounds. It should be noted that these bounds consider all possible patch geometries fitting within the design region Ω , thereby obtaining a fundamental limit on achievable maximum radiation efficiency and gain for antenna geometries within Ω .

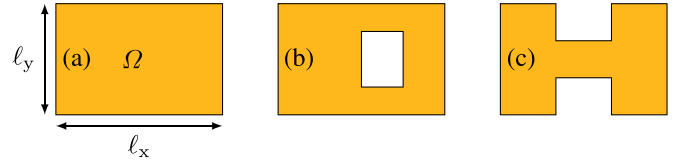


Fig. 2. Rectangular design region Ω , see Fig. 1, having dimensions ℓ_x and ℓ_y is chosen in this article. Classical metal patch geometries such as (a) half-wavelength patch, (b) slot-loaded patch, and (c) H-shaped patch fit within this design region.

Radiation efficiency and gain are defined as [6]

$$\eta = \frac{P_r}{P_d} \quad \text{and} \quad G = 4\pi \frac{U}{P_d}, \quad (1)$$

respectively, where P_r denotes radiated power, P_d dissipated (accepted) power, and U radiation intensity. For a microstrip patch antenna, the dissipated power can be due to three different loss mechanisms that can be separately analyzed as

$$P_d = P_r + P_\Omega + P_\varepsilon \quad (2)$$

where the Ohmic losses on the patch are given by P_Ω and losses in the substrate due to dielectric losses and surface waves are given by P_ε . In reality, the dielectric substrate is always finite, leading to radiation from surface wave diffraction on the edge. However, this form of radiation is generally undesirable and therefore considered as a loss when analyzing radiation efficiency and gain [18]. The remainder of this section focuses on how to analyze the dissipated power, radiation intensity, and radiated power to evaluate the radiation efficiency and gain (1) in a way suitable for current optimization [9]. It should be noted that Ohmic losses on the ground plane are not considered in this article.

For a given microstrip patch antenna geometry and feed, the total dissipated power (P_d) can be determined from the input voltage and current. However, in this article, all possible geometries on a design region need to be considered, and therefore, another approach is required. To formulate a current optimization problem, all patch currents need to be related to dissipated power. This can be done using the method of moments (MoM) [19]. By making use of Green's functions, incorporating the effect of the dielectric substrate and the ground plane [18], the only unknowns of the system are the currents on the design region, see Fig. 1. The current density $J(r)$ in the design region Ω is expanded in N basis functions $\psi_n(r)$ as

$$J(r) = \sum_{n=1}^N I_n \psi_n(r) \quad (3)$$

where the position vector is given by r . The MoM impedance matrix $\mathbf{Z} \in \mathbb{C}^{N \times N}$ relates design region currents to voltages as [19]

$$\mathbf{ZI} = \mathbf{V} \quad (4)$$

where the expansion coefficient I_n are collected in $\mathbf{I} \in \mathbb{C}^{N \times 1}$ and excitation voltages in $\mathbf{V} \in \mathbb{C}^{N \times 1}$. The MoM resistance matrix and reactance matrix are expressed in terms of the

impedance matrix as

$$\mathbf{R} = \frac{\mathbf{Z} + \mathbf{Z}^H}{2} \quad \text{and} \quad \mathbf{X} = \frac{\mathbf{Z} - \mathbf{Z}^H}{2j}, \quad (5)$$

respectively, where the Hermitian transpose is denoted by superscript H and $j^2 = -1$.

The dissipated power (2) required to obtain radiation efficiency and gain (1) can be computed from the patch currents (3) and MoM resistance matrix (5) as [19]

$$P_d = \frac{1}{2} \mathbf{I}^H \mathbf{R} \mathbf{I}. \quad (6)$$

To formulate efficiency and gain optimization problems, it is also required to relate patch currents to radiation intensity and radiated power. For this, analytic expressions of the far-field radiated by a horizontal electric (Hertzian) dipole (HED) located on top of the dielectric slab are used to determine the far-field of the basis functions in (3), see Appendix B for details. This relationship is used to relate the currents to the far-field in any arbitrary direction (θ, ϕ) as

$$\mathbf{F}(\theta, \phi) \approx \mathbf{FI} \quad (7)$$

where the far-field matrix $\mathbf{F} \in \mathbb{C}^{2 \times N}$ relates patch currents to the far-field direction with $\hat{\theta}$ and $\hat{\phi}$ components.

The radiation intensity in a direction (θ, ϕ) used to evaluate gain in (1) is given by

$$U = \frac{|\mathbf{F}|^2}{2Z_0}. \quad (8)$$

From this, the radiated power is calculated by integrating over a hemispherical surface on the free-space side of the design region, neglecting surface wave effects near the grazing angle ($\theta = \pi/2$). Using a set of quadrature points (θ_n, ϕ_n) together with quadrature weights, a matrix \mathbf{F}_s is constructed by using far-field matrices \mathbf{F} in (7) evaluated at (θ_n, ϕ_n) as rows. For simplicity, square roots for the quadrature weights are incorporated into \mathbf{F}_s such that the radiated power P_r from patch currents \mathbf{I} is determined by a radiation resistance matrix $\mathbf{R}_r = \mathbf{F}_s^H \mathbf{F}_s$, i.e.,

$$P_r = \frac{1}{2} \mathbf{I}^H \mathbf{F}_s^H \mathbf{F}_s \mathbf{I} = \frac{1}{2} \mathbf{I}^H \mathbf{R}_r \mathbf{I}. \quad (9)$$

III. BOUNDS ON RADIATION EFFICIENCY AND GAIN

This section formulates and presents upper limits on radiation efficiency and gain using current optimization [7], [20]. Maximal efficiency (1) is in the form of a Rayleigh quotient [19], which can also be written as a quadratically constrained quadratic program (QCQP) [21] as

$$\begin{aligned} & \text{maximize} && \mathbf{I}^H \mathbf{R}_r \mathbf{I} \\ & \text{subject to} && \mathbf{I}^H \mathbf{R} \mathbf{I} = 2P_{in} \end{aligned} \quad (10)$$

where the choice of input power P_{in} does not affect the bounds but only scales the currents. The solution of this optimization problem is in the form of a generalized eigenvalue problem [19] $\eta_{up} = \max \text{eig}(\mathbf{R}_r, \mathbf{R})$.

To enforce self-resonance in the radiation efficiency optimization problem (10), the reactive power is set to zero to model a real-valued input impedance ($\text{Im } Z_{in} = 0$). This

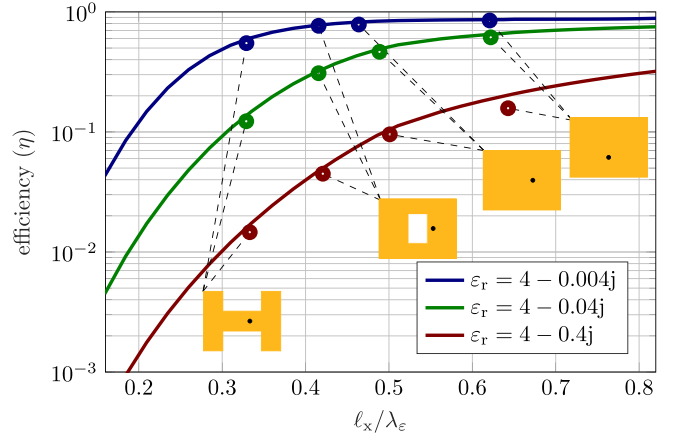


Fig. 3. Upper bounds on radiation efficiency for all PEC microstrip patch antennas fitting within a rectangular design region Ω with dimensions $\ell_y = 0.77\ell_x$ (see Fig. 2) having dielectric loss tangent $\tan \delta \in \{0.001, 0.01, 0.1\}$ and substrate thickness $h = 0.05\ell_x$ (see Fig. 1). Radiation efficiencies computed using FEKO are shown by markers for the indicated patch antenna geometries (see insets (a)–(c) in Fig. 2).

additional reactive power constraint is written as a quadratic form over the reactance matrix (\mathbf{X}) in (5) and reduces the search space of possible optimal currents resulting in the optimization problem

$$\begin{aligned} & \text{maximize} && \mathbf{I}^H \mathbf{R}_r \mathbf{I} \\ & \text{subject to} && \mathbf{I}^H \mathbf{R} \mathbf{I} = 2P_{in} \\ & && \mathbf{I}^H \mathbf{X} \mathbf{I} = 0. \end{aligned} \quad (11)$$

The QCQP (11) can be transformed to a dual problem [20] and written as a parameterized eigenvalue problem using a scalar parameter v . Where, given the condition $\mathbf{R} + v\mathbf{X} \succeq \mathbf{0}$ and an indefinite \mathbf{X} , the scalar parameter is restricted to the range (29) shown in Appendix C. The use of the far-field matrix \mathbf{F}_s in (9) reformulates the solution of (11) as a parameterized ordinary eigenvalue problem, expressed as

$$\eta_{ub} = \min_v \max \text{eig}(\mathbf{F}_s (\mathbf{R} + v\mathbf{X})^{-1} \mathbf{F}_s^H). \quad (12)$$

It should be noted that a simultaneous diagonalization of \mathbf{R} and \mathbf{X} can be used to reduce the computational complexity in (12) by inverting a diagonal matrix [20]. There is typically no dual gap for the QCQPs presented here with one or two quadratic constraints [22]. Therefore, the optimal currents (11) can be determined from eigenvectors in (12).

Fig. 3 shows upper bounds on the radiation efficiency computed for PEC microstrip patch antennas with a dielectric substrate having $\text{Re}\{\epsilon_r\} = 4$ and loss tangent $\tan \delta \in \{0.001, 0.01, 0.1\}$ using (12). The design region Ω has dimensions $\ell_y = 0.77\ell_x$ and substrate thickness $h = 0.05\ell_x$ (see Fig. 1), where again it should be noted that the bounds provide a performance limit for all possible patch geometries within the design region. The bounds are shown for a varying patch length ℓ_x normalized by the dielectric wavelength, $\lambda_\epsilon = \lambda/\sqrt{\text{Re } \epsilon_r}$ (neglecting the imaginary part of permittivity). The bounds are tight from a practical point of view, as shown by the comparison with realistic antennas with an infinite ground plane simulated using commercial software (FEKO)

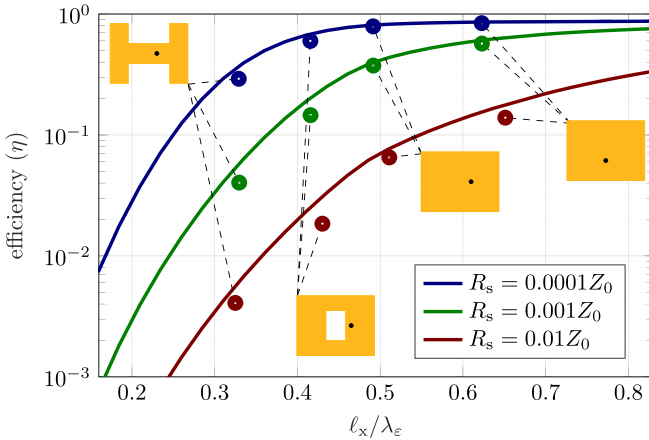


Fig. 4. Upper bounds on the radiation efficiency for all microstrip patch antennas fitting within the rectangular design region with dimensions $\ell_y = 0.77\ell_x$, specified Ohmic losses, relative permittivity $\varepsilon_r = 4$, and substrate thickness $h = 0.05\ell_x$. Radiation efficiencies for the classical patches in Fig. 2 computed using FEKO are shown by markers.

and indicated by the markers to have near-optimal performance. For instance, the half-wavelength patch [see Fig. 2(a)] is shown to be essentially on the bounds for all presented loss tangents, with only a slight deviation from the bounds when exciting the half-wavelength resonance along the shorter dimension (ℓ_y) and increasing the loss tangent to $\tan \delta = 0.1$. However, this deviation could potentially be minimized with a different feeding configuration. Considering miniaturized geometries, performance near the bounds is also observed for the slot-loaded patch [see Fig. 2(b)] as well as the H-shaped patch [see Fig. 2(c)].

The results in Fig. 3, as expected, show that when the dielectric loss tangent is decreased or the electrical size is increased, the maximum radiation efficiency increases. For design regions smaller than half a wavelength in the dielectric ($\ell_x/\lambda_\epsilon < 0.5$), the bounds show that for a high loss tangent, e.g., $\tan \delta = 0.1$ miniaturized designs perform relatively poorly. To demonstrate this, compare the bounds for $\tan \delta = 0.1$ at $\ell_x/\lambda_\epsilon \approx 1/3$ (realized by the H-shaped patch) around 1.5% efficiency and $\ell_x/\lambda_\epsilon \approx 1/2$ (realized by half wavelength patch) around 10% efficiency. For a loss tangent $\tan \delta = 0.001$, the same comparison leads to bounds at $\ell_x/\lambda_\epsilon \approx 1/3$ of around 60% and at $\ell_x/\lambda_\epsilon \approx 1/2$ around 80%. This emphasizes the importance of choosing a substrate with low dielectric losses when considering antennas that are smaller than half a wavelength in the dielectric. It should be noted that further improvements in radiation can be achieved using designs larger than $\ell_x/\lambda_\epsilon > 0.5$. This is done by exciting a half wavelength resonance on the shorter dimension (ℓ_y) as is well known. This is confirmed by both the bounds and the simulated patch antennas.

Radiation efficiency bounds computed using (12) for patches with varying surface resistivity $R_s \in \{0.0377, 0.377, 3.77\} \Omega/\square$ (ohms per square) and a lossless dielectric are shown in Fig. 4. The surface resistivity can model either a resistive sheet or a solid conductor with a skin depth [23]. To demonstrate the practical application of the bounds, the performance of different patch designs (see Fig. 2), is compared to

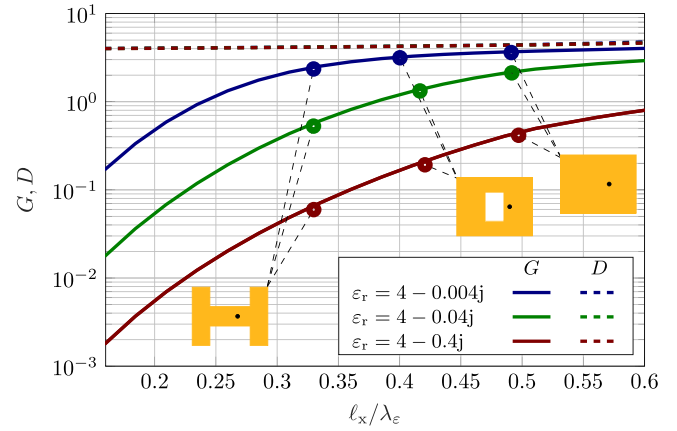


Fig. 5. Upper bounds on the gain in the normal direction, \hat{z} , for microstrip patch antennas fitting within a rectangular design region with dimensions $\ell_y = 0.77\ell_x$, relative permittivity $\text{Re}\{\varepsilon_r\} = 4$, loss tangents $\tan \delta \in \{0.001, 0.01, 0.1\}$, and substrate thickness $h = 0.05\ell_x$. The corresponding realized directivities are shown by dashed lines.

the bounds using FEKO. This shows that the half-wavelength-patches [see Fig. 2(a)] are essentially on the bounds and, therefore, optimal for these surface resistivities. Further, the slot-loaded patch [see Fig. 2(b)] and H-shaped patch [see Fig. 2(c)] perform near the bounds. The reason the slot-loaded patch and the H-shaped patch do not align with the bounds is that the currents are constrained in these designs, leading to high current densities resulting in less efficient use of the available surface area. Similar to Fig. 3, it is observed that increasing design region dimensions may be used to compensate for high losses.

A further parameter of interest is gain (1). Upper bounds on gain can be determined by maximization of the radiation intensity and written as the current optimization problem

$$\begin{aligned} &\text{maximize} && \mathbf{I}^H \mathbf{F}^H \mathbf{F} \mathbf{I} \\ &\text{subject to} && \mathbf{I}^H \mathbf{R} \mathbf{I} = 2P_{\text{in}} \\ & && \mathbf{I}^H \mathbf{X} \mathbf{I} = 0 \end{aligned} \quad (13)$$

which can be formulated as an eigenvalue problem (see Appendix C for more information) using the range computed for v in (29) as [20]

$$G_{\text{ub},r} \approx 4\pi \min_v \max \text{eig}(\mathbf{F}(\mathbf{R} + v\mathbf{X})^{-1} \mathbf{F}^H). \quad (14)$$

Upper bounds on gain for microstrip patch antennas with relative permittivity having real part $\text{Re}\{\varepsilon_r\} = 4$, varying loss tangent, substrate thickness $h = 0.05\ell_x$, and design region dimensions $\ell_y = 0.77\ell_x$ are shown in Fig. 5. The bounds show that, as expected, an increased dielectric loss tangent reduces the gain. Further, the corresponding directivity ($D = G/\eta$) values, shown by dashed lines, are on top of one another with only a weak dependence on the electrical size of the design region. This suggests that the maximum achievable gain is scaled by achievable radiation efficiency with directivity relatively unaffected. The gain bounds on Ohmic losses are not shown here, however, they lead to the same conclusion on directivity as the bounds with dielectric losses presented in Fig. 5. This suggests that directivity is mostly determined by the electrical size of the structure when maximizing gain.

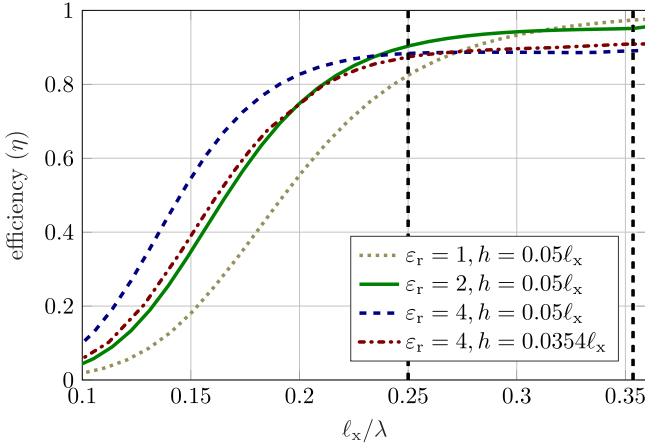


Fig. 6. Upper bounds on radiation efficiency with surface resistivity $R_s = 0.01 \Omega/\square$. The design region has dimensions $\ell_y = 0.77\ell_x$, substrate thickness h , and relative permittivity ϵ_r as indicated in the legend. The vertical dashed lines indicate the half wavelength size for substrates with relative permittivity of 2 and 4.

IV. SUBSTRATE IMPACT ON ANTENNA MINIATURIZATION

In this section, the trade-off between antenna miniaturization and radiation efficiency bounds is investigated. Miniaturizing patch antennas can be achieved by increasing the substrate's relative permittivity and/or shaping the patch geometry. A comparison between these two approaches for a given design region and free-space wavelength is provided here. This is done for a design region with dimensions $\ell_y = 0.77\ell_x$, substrate thickness $h = 0.05\ell_x$, and relative permittivities $\text{Re}\{\epsilon_r\} = 2$ and $\text{Re}\{\epsilon_r\} = 4$, investigating Ohmic as well as dielectric losses separately. In addition, the radiation efficiency bounds are compared to measurements of miniaturized patch antennas for a given substrate.

A comparison of the efficiency bounds for different substrate relative permittivities is shown in Fig. 6 for patch Ohmic losses of $R_s = 0.01 \Omega/\square$ (similar to copper at $f = 1$ GHz) and lossless dielectrics. It is evident that the higher relative permittivity substrate ($\epsilon_r = 4$) has greater radiation efficiency bounds than the lower permittivity ($\epsilon_r = 1$ and $\epsilon_r = 2$) substrates, for structures miniaturized below its half a wavelength (in the $\epsilon_r = 4$ substrate) $\ell_x/\lambda < 0.25$. The enhanced efficiency of the high permittivity substrate ($\epsilon_r = 4$) can be attributed in part to its greater electrical thickness. This is demonstrated by comparing its efficiency bound with that of a thinner substrate, $h = 0.0354\ell_x$, equivalent to the electrical thickness of the $\epsilon_r = 2$ material. The results indicate that the substrate's electrical thickness is a critical factor in determining efficiency bounds for designs smaller than half a wavelength.

The performance differences among the various substrates become less pronounced for $\ell_x/\lambda > 0.25$, where all scenarios exhibit efficiencies ranging from around 85%–95%. The $\epsilon_r = 2$ substrate demonstrates marginally better performance up to $\ell_x/\lambda \approx 0.3$, beyond which the free-space scenario ($\epsilon_r = 1$) excels. In this range, efficiency bounds for the two $\epsilon_r = 4$ substrates are comparable, with slightly better performance observed for the thinner substrate. The intricate behavior within this range arises from a combination of increased

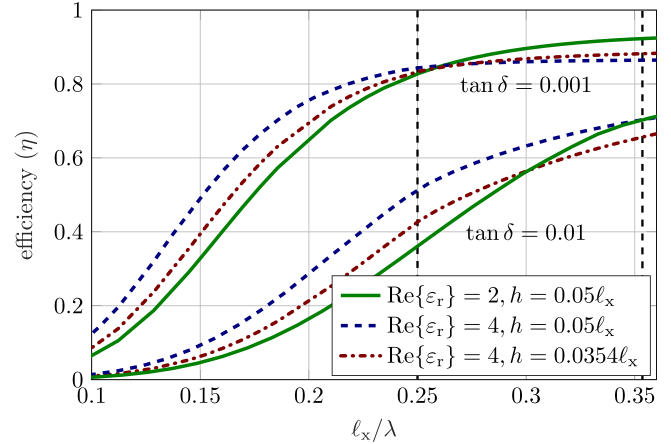


Fig. 7. Upper bounds on radiation efficiency for two relative permittivities with substrate loss tangents $\tan \delta \in [0.01, 0.001]$. The design region has dimensions $\ell_y = 0.77\ell_x$ and indicated substrate thickness h and relative permittivity ϵ_r in the legend. The vertical dashed lines indicate the half wavelength size for substrates with relative permittivity of 2 and 4.

electrical size and increased surface wave losses for the higher permittivity substrates.

Further, considering only dielectric losses, the radiation efficiency bounds for relative permittivity $\epsilon_r = 2(1 - j \tan \delta)$ and $\epsilon_r = 4(1 - j \tan \delta)$ substrates are compared as shown in Fig. 7. The interpretation remains consistent for the low-loss substrate with $\tan \delta = 0.001$, similar to the Ohmic losses depicted in Fig. 6. Specifically, the high permittivity substrate ($\text{Re}\{\epsilon_r\} = 4$) exhibits the highest efficiency bound below $\ell_x/\lambda < 0.25$, while the lower permittivity substrate ($\text{Re}\{\epsilon_r\} = 2$) outperforms it above $\ell_x/\lambda > 0.25$. Once more, this phenomenon primarily stems from the larger electrical size in electrically small cases and the increased surface wave power for larger sizes. Using a thinner substrate of $h = 0.0354\ell_x$ reduces the efficiency, bringing the values closer to those of the $\text{Re}\{\epsilon_r\} = 2$ case, although with a disparity larger than observed for the Ohmic losses in Fig. 6.

In the case of higher dielectric losses with $\tan \delta = 0.01$, the higher permittivity substrate exhibits superior performance across the entire range $\ell_x/\lambda < 0.36$. This can be attributed in part to the dominance of material losses, which hide the impact of surface waves, resulting in lower efficiency overall. Furthermore, the enhancement observed beyond the dielectric's half a wavelength, $\ell_x/\lambda > 0.25$, is attributable to the fact that the ℓ_y -direction becomes half a wavelength increasing the width of the patch.

Based on these investigations, it is recommended that when considering miniaturization, a higher permittivity substrate should be preferred over reshaping the design region. The exact range over which it remains favorable to do so depends on several factors such as surface wave losses. From the cases considered here, it is observed that for low-loss cases, it is favorable to miniaturize by increasing relative permittivity up to around half a wavelength. To better understand this, a further study of how the surface wave depends on design parameters is presented in Section V.

For a given dielectric substrate, the bounds can be compared to measured antenna designs. This is both a validation of the

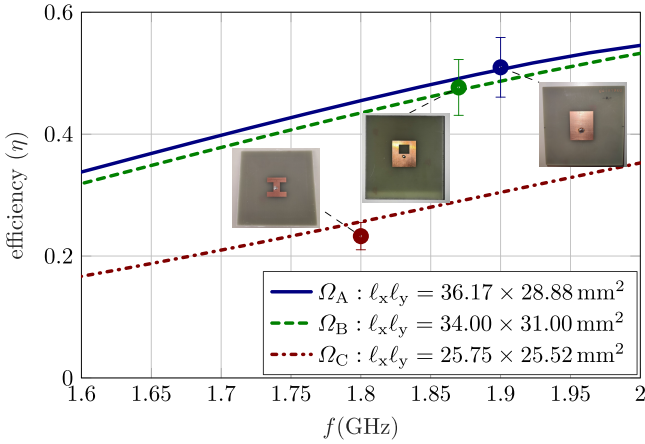


Fig. 8. Upper bounds on radiation efficiency compared with measurements. The efficiency of three measured antennas is shown with markers. The design region's dimensions are given in the legend. The relative permittivity of the $h = 3.3$ mm thick substrate is $\epsilon_r = 4.29(1 - j0.015)$ and the used surface resistivity of copper is $R_s = 0.01 \Omega/\square$. Error bars are based on the precision of the measurement. The ground plane has dimensions $100 \text{ mm} \times 100 \text{ mm}$.

bounds' usefulness for a finite ground plane as well as an investigation of miniaturized designs on the same dielectric substrate. The FR4 dielectric substrate chosen has dimensions $100 \text{ mm} \times 100 \text{ mm}$ with thickness 3.3 mm and relative permittivity $\epsilon_r \approx 4.29(1 - j0.015)$, based on material characterization at 2 GHz [24]. Three different design regions are considered and their radiation efficiency bounds determined for $1.6\text{--}2 \text{ GHz}$ as indicated in Fig. 8. The smallest design region (Ω_C) has significantly lower radiation efficiency bounds than the other two design regions (Ω_A and Ω_B). When comparing the two largest design regions, the one with the largest maximum dimension has higher radiation efficiency bounds, confirming that for miniaturized geometries it is generally favorable to increase the largest dimension.

Since a finite ground plane is used, part of the undesired surface wave power is detected as radiated power in the measurement. However, since the ground plane is relatively large compared to the design region, the bounds should still be a good indication of optimal performance [2]. Should the surface wave have a larger effect on the radiation efficiency, such as in the case of an electrically thicker dielectric substrate, then this should be accounted for. When comparing the half-wavelength patch with design dimensions Ω_A at 1.9 GHz to the bounds, the measured radiation efficiency is found to be very close to these bounds. Similarly, for the slot-loaded patch (designed within the design region Ω_B), the measured radiation efficiency is close to the bounds at 1.87 GHz . The H-shaped patch (designed within the design region Ω_C) has a slight deviation from the bounds at 1.8 GHz .

V. SEMI-ANALYTIC APPROXIMATION OF BOUNDS

In this section, the contribution of substrate and patch loss parameters pertaining to radiation efficiency bounds are further investigated, to see if this effect can be approximated to enhance understanding and simplify computations. With this, insights can be derived into how the substrate or patch material properties affect the radiation efficiency bounds.

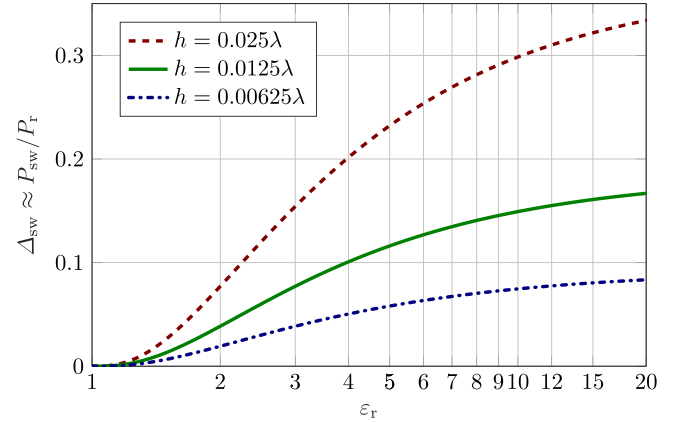


Fig. 9. Ratio between the first surface wave mode power (P_{sw}) and radiated power (P_r) for an HED approximated by (16). The expression is evaluated over a range of relative permittivities and for three electrical thicknesses.

The dissipation factor [6], [7], defined as

$$\Delta = \frac{P_d - P_r}{P_r} = \frac{P_\varepsilon + P_\Omega}{P_r} \quad (15)$$

is a natural parameter to consider when investigating the effect of loss parameters on the scaling of radiation efficiency bounds [obtained with (12)]. The dissipation factor is related to the radiation efficiency as $\eta = (1 + \Delta)^{-1}$. Therefore, upper bounds on radiation efficiency provide lower bounds on dissipation factor.

As shown in [7] for antennas in free space, lower bounds on dissipation factor scale linearly with surface resistivity (R_s). However, only considering this scaling for microstrip patch antennas does not account for surface wave effects, as, even with lossless materials, $P_\varepsilon \neq 0$. To account for this effect, an approximate expression [25]

$$\frac{P_{sw}}{P_r} \approx \Delta_{sw} = \frac{3\pi}{4} \frac{(\text{Re}\{\epsilon_r\} - 1)^3 kh}{\text{Re}\{\epsilon_r\}^2(\text{Re}\{\epsilon_r\} - 1) + \frac{2}{5} \text{Re}\{\epsilon_r\}} \quad (16)$$

relating the surface wave power to the radiated power of a HED is used, see Fig. 9. The surface wave is strictly only defined for lossless dielectrics, but in (16), it is assumed that the ratio between propagated power in the dielectric and radiated power (9) remains constant with increased loss tangent. Further, due to the choice of thin dielectric substrates, only the first transverse magnetic surface wave mode is propagating [26]. The thickness required to have the first transverse electric surface wave mode propagating in the substrate is $h > \lambda/(4\sqrt{\epsilon_r - 1})$ [18] in a lossless substrate. It should be noted that with a finite ground plane, the surface wave (16) introduces edge diffraction, which alters the main lobe of the radiation pattern and leads to the formation of sidelobes and increased back radiation, particularly in the E-plane [2].

For three electrical thicknesses over a range of relative permittivities, the expression (16) is used to approximate the surface wave to radiated power ratio as shown in Fig. 9. In the figure, the $h = 0.0125\lambda$ at $\epsilon_r = 4$ corresponds to a relative permittivity of 4 substrate at half a dielectric wavelength in Figs. 3 and 4. It should be noted that by increasing the relative permittivity higher order surface wave modes could be excited, although this is not the case in Fig. 9.

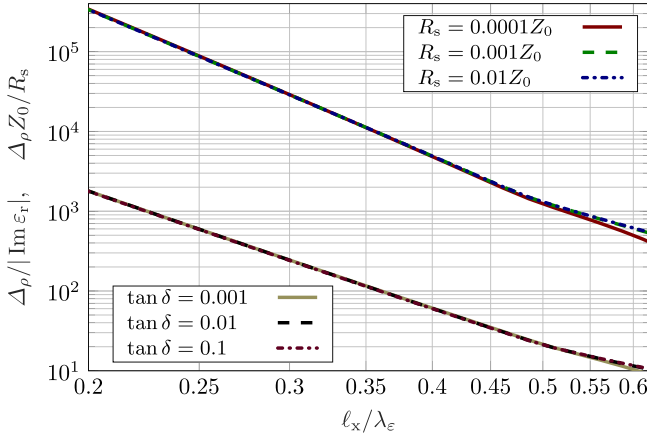


Fig. 10. Lower dissipation factor (17) bounds with the surface wave contribution (16) subtracted. The bounds are shown for different surface resistivities normalized by surface resistivity and different dielectric loss tangents normalized by the imaginary part of permittivity. The substrate relative permittivity is $\text{Re}\{\epsilon_r\} = 4$, thickness $h = 0.05\ell_x$, and the patch region dimensions are $\ell_y = 0.77\ell_x$.

The normalized surface wave power (16) can be approximately removed from the dissipation factor (15) as

$$\Delta_\rho = \Delta - \Delta_{sw}. \quad (17)$$

This is applied to the lower dissipation factor bounds obtained using (12), along with normalizing with the surface resistivity ($\Delta_\rho Z_0 / R_s$), as shown in Fig. 10. The results show very little difference between the bounds for the different resistivities R_s when removing the two main contributions (surface resistivity and surface wave). It is noted that as the electrical size increases, the bounds start to deviate slightly. This is due to the surface wave approximation (16) not being accurate for these cases [25] along with the optimal currents trying to suppress these losses as they become more significant. It is very important to note that (16) does not indicate a bound on the ratio between surface wave and radiated power. However, it is an excellent approximation when the surface wave power is not a dominant contribution to radiation efficiency as confirmed in Fig. 10.

To investigate the bounds' dependence on dielectric losses, the relationship between dissipated power in the dielectric substrate and the imaginary part of the relative permittivity is required. This is given by

$$P_e = \frac{-1}{2} \int \text{Im}\{\epsilon_r(\mathbf{r})\} |\mathbf{E}(\mathbf{r})|^2 dV \quad (18)$$

where it is sufficient to integrate over the volume of the substrate. Assuming that the nonpropagating (excluding surface waves) part of the electric field in the substrate remains constant when the dielectric losses are increased, then the dissipation factor (15) should scale linearly with respect to the dielectric losses (18), neglecting the surface wave. Further, as only the real part of the relative permittivity is taken in (16), the ratio between radiated and surface wave power is assumed to remain constant.

The normalized lower bounds on the dissipation factor for varying dielectric loss tangents are shown in Fig. 10. The bounds with this normalization, along with subtracting the

surface wave power (16), are approximately equal for all presented loss tangents. This means that the lower dissipation factor bounds scale approximately linearly with respect to loss tangent after the approximate surface wave power is removed, implying negligible changes to the near field. Further, the ratio of surface wave power to radiated power approximately follows (16) except for electrically large patches.

VI. CLOSED FORM EXPRESSION OF MAXIMUM RADIATION EFFICIENCY LINKED TO MINIMUM Q-FACTOR

In this section, a link between stored electric energy in the substrate and dielectric losses is established [27]. This allows for the microstrip patch antenna Q-factor to be related to its radiation efficiency leading to a link between maximum radiation efficiency and minimum Q-factor (maximum bandwidth). This link requires that most of the stored electric energy is confined in the dielectric substrate similar to the assumption made in the cavity model [3]. With this assumption, the stored electric energy can be related to the dissipated power in the near field (due to dielectric substrate losses) and along with surface wave power (16) can be related to the total dissipated power in the substrate as

$$P_e \approx 2\omega W_e \tan \delta + P_{sw} \quad (19)$$

where the stored electric energy is given by W_e . Adding the radiated power to (19) and using the total dissipated power (2), leads to

$$P_d \approx P_r + P_{sw} + 2\omega W_e \tan \delta \quad (20)$$

assuming no Ohmic losses. It is useful to rewrite (20) in terms of the Q-factor that can be approximated from the fractional bandwidth or input impedance frequency derivative [28] as shown in Appendix D. This can easily be measured with e.g., a VNA.

Self-resonant antennas have equal stored electric and magnetic energies, which simplifies the Q-factor [28] to

$$Q = \frac{2\omega W_e}{P_d}. \quad (21)$$

Substituting the Q-factor (21) into (20) normalized by dissipated power and identification of the efficiency (1) yields

$$1 \approx \eta + \frac{P_{sw}}{P_d} + Q \tan \delta. \quad (22)$$

Using the approximation (16) for the surface wave power, the radiation efficiency can be factored out in (22) and expressed as

$$\eta \approx \frac{1 - Q \tan \delta}{1 + \Delta_{sw}}. \quad (23)$$

Assuming the ratio of surface wave power to radiated power (Δ_{sw}) remains constant when the loss tangent is increased, it is clear from (23) that minimizing Q-factor is equivalent to maximizing radiation efficiency. This means that maximizing bandwidth and radiation efficiency are closely related for self-resonant microstrip patch antennas.

Lower Q-factor bounds of a lossless substrate can be related to maximum radiation efficiency [29] of a lossy substrate when

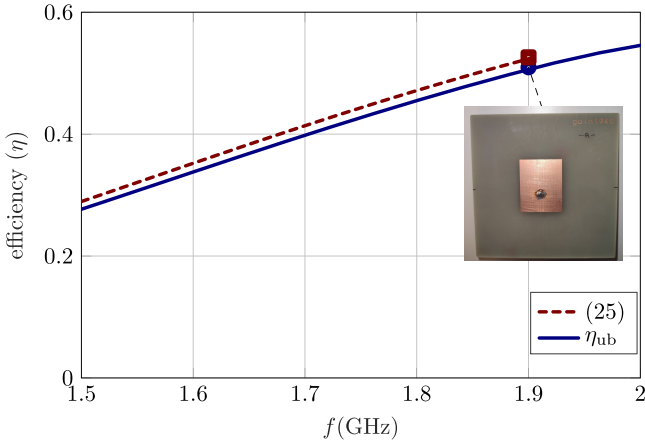


Fig. 11. Upper bounds on radiation efficiency determined using current optimization (12) compared to an approximation of the bounds from the Q-factor (25). The Q-factor is determined from a measured half-wavelength microstrip patch antenna with relative permittivity $\varepsilon_r = 4.29(1 - j0.015)$, substrate thickness $h = 3.3\text{ mm}$, design region dimensions $\ell_x \ell_y = 36.17 \times 28.88\text{ mm}^2$, and the ground plane has dimensions $100\text{ mm} \times 100\text{ mm}$.

the radiated Q-factor (Q/η) is assumed to be invariant with respect to loss tangent, as suggested by results presented in Fig. 10. The lower Q-factor bounds for a patch antenna on a lossless substrate (Q_{lb}) are here defined in terms of the Q-factor of a half wavelength patch (Q_{hw}) with dielectric losses as

$$Q_{lb} = \frac{Q_{hw}}{\eta(1 + \Delta_{sw})}. \quad (24)$$

Substituting this into the expression relating efficiency to Q-factor (23) leads to an approximation of maximum radiation efficiency in terms of the lower Q-factor bound for a patch antenna on a lossless substrate as

$$\eta_{ub} \approx \frac{1}{(Q_{lb} \tan \delta + 1)(\Delta_{sw} + 1)}. \quad (25)$$

The lower Q-factor bounds in this expression can be determined from results presented in [10] by comparing the result with the maximum radiation efficiency obtained from (12).

The steps required to approximate radiation efficiency bounds from the Q-factor of a single half-wavelength patch antenna assuming negligible Ohmic losses are outlined in Appendix E. This can be useful as the Q-factor can be determined from measurements and simulations. The results, as shown in Fig. 11, indicate that lower Q-factor bounds of a microstrip patch antenna are a good approximation of maximum achievable radiation efficiency when dielectric losses are added. Further, applying a scaling rule, the measured results can be used to approximate the maximum achievable radiation efficiency for miniaturized designs as shown by the dashed line in Fig. 11.

In [3], the Q-factor is linked to Ohmic losses of half wavelength microstrip patch antennas by using the cavity model approximation. This can be used to write a similar expression to (25) for only Ohmic losses by replacing $\tan \delta$ in (25) with $2R_s/(khZ_0)$. This assumes Ohmic losses on both the ground plane and patch. The assumption made here of only

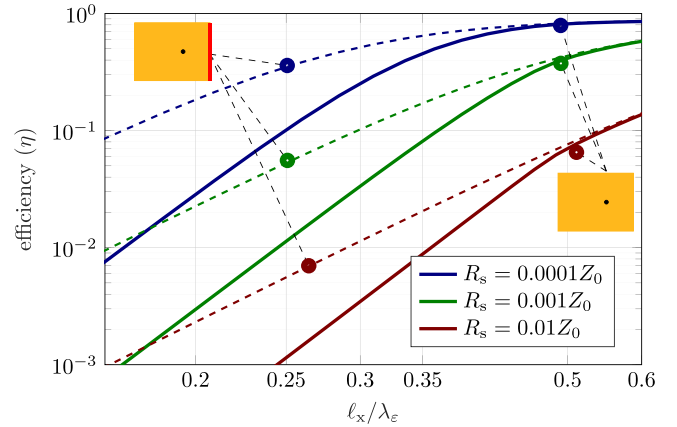


Fig. 12. Upper bounds on radiation efficiency compared with (11) (solid) and without (10) (dashed) self-resonant constraint. The bounds are given for varying surface resistivities. Along with the performance of half-wavelength patch antennas, some PIFAs' radiation efficiency is also shown. The side of the PIFAs shorted to the ground is indicated with red. The design region dimensions are $\ell_y = 0.77\ell_x$, the substrate thickness is $h = 0.05\ell_x$, and the relative permittivity is $\varepsilon_r = 4$.

Ohmic losses on the patch region can be made by replacing $R_s/(khZ_0)$ instead. This expression is expected to be less accurate than (25) as the stored energy is less clearly linked to Ohmic losses in a general setting.

VII. VERTICAL CURRENTS

In this article, the bounds constraints do not consider vertical currents between the ground plane and the dielectric substrate. However, it is worth noting an interesting miniaturization approach, consisting of using a shorting pin/wall to miniaturize the patch [12]. This avoids having to reshape the rectangular metal design region into, for instance, an H-shaped patch [see Fig. 2(c)] but requires the addition of vias, leading to planar inverted-F antenna (PIFA) designs. These antennas can be simulated in commercial software using a shorting wall, as shown in Fig. 12, demonstrating significantly higher radiation efficiency compared to the self-resonant bounds. To better understand the reason for this discrepancy, the self-resonant constraint is removed (10), demonstrating significantly higher radiation efficiency compared to the self-resonant bounds below half a wavelength. This leads to bounds performance similar to the PIFA radiation efficiency, suggesting that PIFA antennas essentially make the optimal Ohmic loss patch currents self-resonant. It should be noted that the PIFA also performs better than the self-resonant dielectric loss bounds. However, when the self-resonant constraint is removed, highly inductive loop currents that do not radiate in the normal direction and produce high Ohmic losses, lead to significantly higher radiation efficiency bounds.

VIII. CONCLUSION

This article investigates the performance limitations of microstrip patch antennas by presenting radiation efficiency and gain bounds. These bounds provide a realistic benchmark for assessing the feasibility and evaluating trade-offs involved in antenna design. Through a comprehensive study,

the close alignment of these theoretical bounds with practical designs is demonstrated, highlighting their practical relevance. This closeness has been challenging to achieve on previous formulations of radiation efficiency bounds, especially for miniaturized designs [20]. The article also presents a relationship between maximum bandwidth and maximum radiation efficiency, which could be very useful in the design process.

The following key findings summarize the contributions of this work.

- 1) The radiation efficiency and gain bounds presented in this article are shown to be close to the practical microstrip patch antenna design's performance. This emphasizes the usefulness of these bounds as they serve as a realistic benchmark to assess feasibility and evaluate trade-offs.
- 2) The bounds highlight the performance trade-offs linked to patch miniaturization, indicating that utilizing a higher permittivity substrate is often more beneficial than reshaping the patch design region for miniaturization.
- 3) Since the formulation for obtaining the bounds is not currently available in commercial solvers, an approximation is derived using the performance of a single half-wavelength patch antenna. This allows the antenna design community to utilize the bounds when considering the miniaturization of microstrip patch antennas.
- 4) The bounds are further used to present an approximate relationship between maximum bandwidth (minimum Q-factor) and maximum radiation efficiency. This new finding suggests that in many instances, optimizing one of these parameters also implicitly optimizes the other.

This study makes significant advancements in understanding the performance limits of microstrip patch antennas. By establishing these bounds, a valuable tool for antenna designers is provided to benchmark their designs against the theoretical limits. The close agreement between the bounds and practical designs underscores their relevance and utility. However, future research should focus on addressing the remaining open questions, including the effects of finite ground planes and the inclusion of vertical currents in the bounds formulation. These investigations will further refine the bounds and extend their applicability, ultimately aiding in the development of more efficient and effective antenna designs.

APPENDIX A NOTATION USED

In Table I, a summary of the notation used in the article is provided.

APPENDIX B FAR-FIELD EXPRESSIONS

The current density $\mathbf{J}(\mathbf{r})$ in (3) in the design region is related to the radiated power by integration of the radiation intensity. Linked to the radiation intensity is the far-field, $\mathbf{F} = F_\theta \hat{\theta} + F_\phi \hat{\phi}$, that is defined in terms of the electric field ($r e^{ikr} \mathbf{E}$) by letting the radial distance $r \rightarrow \infty$ using spherical coordinates, where the elevation angle is given by $\theta \in [0, \pi/2]$

TABLE I
DEFINITIONS OF FREQUENTLY USED PARAMETERS IN THE ARTICLE

Parameter	Definition	Eqn/Fig
η	Radiation efficiency	(1)
G	Gain	(1)
P_r	Radiated power	(1)
P_d	Dissipated power	(1)
P_Ω	Ohmic losses	(2)
P_ϵ	Dielectric losses	(2)
Ω	Design region	(3)
h	Substrate thickness	Fig. 1
ϵ_r	Relative permittivity	Fig. 1
$\mathbf{J}(\mathbf{r})$	Current density	(3)
\mathbf{I}	patch currents	(4)
\mathbf{Z}	MoM impedance matrix	(4)
\mathbf{R}	Resistance matrix	(5)
\mathbf{X}	Reactance matrix	(5)
\mathbf{F}_s	Far-field matrix	(7)
\mathbf{R}_r	Radiation resistance	(9)

and the azimuthal angle is given by $\phi \in [0, 2\pi]$, with the coordinate system shown in Fig. 1.

The far-field contribution from an \hat{x} -directed HED with dipole moment J_h (having units Am) is [18]

$$\begin{aligned} F_\theta &= \frac{Z_0}{2\pi} \frac{-J_h k n_\theta \cos \phi \cos \theta}{n_\theta - j \epsilon_r \cos \theta \cot(k h n_\theta)} \\ F_\phi &= \frac{Z_0}{2\pi} \frac{J_h k \sin \phi \cos \theta}{\cos \theta - j n_\theta \cot(k h n_\theta)} \end{aligned} \quad (26)$$

where Z_0 is the free space impedance and $n_\theta = \sqrt{\epsilon_r - \sin^2 \theta}$. A simple coordinate rotation can be used to calculate the far-field from a \hat{y} -directed HED. It should be noted that (26) was derived for a lossless dielectric substrate [18] and is here extended to the case of lossy substrates. These expressions can be shown to also be valid for lossy dielectric substrates and can alternatively be derived using reciprocity [30].

APPENDIX C OPTIMIZATION FORMULATION

The upper bound on efficiency is determined by multiplying the second constraint in the QCQP (11) with a scalar parameter ν and adding the two constraints $\mathbf{I}^H \nu \mathbf{XI} = 0$ and $\mathbf{I}^H \mathbf{RI} = 2P_{in}$ which yields

$$\begin{aligned} \min_{\nu} \max_{\mathbf{I}} \quad & \mathbf{I}^H \mathbf{R}_r \mathbf{I} \\ \text{subject to} \quad & \mathbf{I}^H (\mathbf{R} + \nu \mathbf{X}) \mathbf{I} = 2P_{in}. \end{aligned} \quad (27)$$

This problem is in the form of a Rayleigh quotient [7] and solved as a parametrized eigenvalue problem

$$\eta_{ub} = \min_{\nu} \max_{\mathbf{I}} \text{eig}(\mathbf{R}_r, \mathbf{R} + \nu \mathbf{X}) \quad (28)$$

where given the condition $\mathbf{R} + \nu \mathbf{X} \succeq \mathbf{0}$ and an indefinite \mathbf{X} , the scalar parameter is restricted to the range

$$\frac{-1}{\max \xi_a} \leq \nu \leq \frac{-1}{\min \xi_a} \quad (29)$$

where $\xi_a = \text{eig}(\mathbf{X}, \mathbf{R})$, resembles characteristic modes [31]. The far-field matrix \mathbf{F}_s (9) is finally used to rewrite (28) as the ordinary eigenvalue problem (12).

The upper bound on gain based on solving (14) may present some challenges in recovering the optimal currents from the eigenvectors to test for no dual gap or calculation of the directivity. To avoid this, the first constraint in (13) can be added to the objective and then rewritten as an eigenvalue problem similar to (28). It should be noted that, for all optimization problems presented here, the problem can be reformulated to only search for solutions with radiating currents to improve numerical stability. Further, using semidefinite programming (SDP), the bounds can be computed in an alternative way [21].

APPENDIX D Q-FACTOR

Q-factor can be approximated from the fractional bandwidth B_{Γ_0} in the case of a single resonance as [28]

$$Q \approx \frac{2}{B_{\Gamma_0}} \frac{\Gamma_0}{\sqrt{1 - \Gamma_0^2}} \quad (30)$$

where Γ_0 is the chosen reflection coefficient threshold. The frequency derivative of the input impedance can also be used to approximate the Q-factor as [28]

$$Q \approx \frac{\sqrt{(\omega R'_{in})^2 + (\omega X'_{in} + |X_{in}|)^2}}{2R_{in}} \quad (31)$$

where the angular frequency derivative is given by ' and R_{in} and X_{in} are the real and imaginary parts of the input impedance, respectively.

APPENDIX E RELATION BETWEEN Q-FACTOR AND RADIATION EFFICIENCY

This appendix outlines the steps to go from the Q-factor of a lossy substrate to an approximation of the maximum radiation efficiency of a miniaturized design region and provides a practical example. Here, the Q-factor is obtained from a half-wavelength patch measurement, however, a simulation could also have been used. Since the dielectric losses are relatively high using an FR4 substrate, the Ohmic losses are ignored when going from Q-factor to radiation efficiency in the following example.

To illustrate the practical use of the expressions in Section VI on how to use the Q-factor of a half wavelength patch antenna to approximate the maximum achievable radiation efficiency for a miniaturized design region, the following steps are used:

- 1) Measure Q-factor of half wavelength patch, e.g., from bandwidth (30) or impedance (31) [28].
- 2) Approximate the ratio of surface wave power to radiated power using (16).
- 3) Determine the approximate radiation efficiency using (23).
- 4) Determine the approximate lossless substrate Q-factor using $Q_{lb} = Q/(1 - Q \tan \delta)$.
- 5) Scale the Q-factor [10].
- 6) Compute new approximate surface wave to radiated power ratio using (16).

- 7) Convert scaled Q-factor to approximate radiation efficiency bounds using (25).

As a practical example, using the half wavelength patch in Fig. 11, resonant at 1.9 GHz these steps can be demonstrated. This design region has dimensions $\ell_x = 36.17$ mm ($\ell_x/\lambda_e = 0.476$), $\ell_y = 28.88$ mm and $h = 3.3$ mm. The substrate relative permittivity is $\epsilon_r = 4.29(1 - j0.015)$. For step 1, the Q-factor of this patch antenna is determined from its fractional bandwidth to be $Q_{hw} = 25.4$ (approximately the same value can be obtained from the input impedance frequency derivative). Then, in step 2, the surface wave power to radiated power ratio is determined from (16) to be $\Delta_{sw} = 0.178$. Using the first two steps, in step 3, the approximate radiation efficiency of the half wavelength patch is calculated from (23). The resulting approximate efficiency is $\eta \approx 0.526$. This radiation efficiency approximation is added to the bounds shown in Fig. 11 and shows a near-optimal value compared to the bounds. Step 4 is then to approximately converted to the Q-factor with dielectric losses removed. This leads to $Q_{lb} = 41$. It may be of interest to assess what the expected approximate maximum radiation efficiency will be miniaturizing to 1.5 GHz with the same design parameters. Then, in step 5, scaling the Q-factor to this frequency, the approximate lower bounds are $Q_{lb} \approx 135.4$. Now, the approximate surface wave to radiated power is calculated in step 6 as $\Delta_{sw} = 0.14$. Finally, in step 7, the approximate achievable radiation efficiency at 1.5 GHz is $\eta \approx 0.29$. The approximated bounds between these two points are approximated by a dashed line.

ACKNOWLEDGMENT

The authors would like to thank Hannes Bartle and Dr. Ismael Triviño from EPFL for helping with the measurements.

REFERENCES

- [1] D. M. Pozar, "Microstrip antenna," *Proc. IEEE*, vol. 80, no. 1, pp. 79–91, Jan. 1992.
- [2] R. Garg, P. Bhartia, I. Bahl, and A. Ittipiboon, *Microstrip Antenna Design Handbook*. Norwood, MA, USA: Artech House, 2001.
- [3] J. R. James and P. S. Hall, *Handbook of Microstrip Antennas*. London, U.K.: Peregrinus on Behalf of the Institution of Electrical Engineers, 1989.
- [4] (2022). FEKO. Altair. [Online]. Available: <https://altairhyperworks.com/product/Feko>
- [5] (2022). CST Studio Suite 3D EM Simulation and Analysis Software. [Online]. Available: <https://www.cst.com/>
- [6] R. F. Harrington, "Effect of antenna size on gain, bandwidth, and efficiency," *J. Res. Nat. Bur. Standards D, Radio Propag.*, vol. 64D, no. 1, pp. 1–12, Jan. 1960.
- [7] M. Gustafsson, M. Capek, and K. Schab, "Tradeoff between antenna efficiency and Q-factor," *IEEE Trans. Antennas Propag.*, vol. 67, no. 4, pp. 2482–2493, Apr. 2019.
- [8] L. Jelinek and M. Capek, "Optimal currents on arbitrarily shaped surfaces," *IEEE Trans. Antennas Propag.*, vol. 65, no. 1, pp. 329–341, Jan. 2017.
- [9] M. Gustafsson and S. Nordebo, "Optimal antenna currents for Q, superdirective, and radiation patterns using convex optimization," *IEEE Trans. Antennas Propag.*, vol. 61, no. 3, pp. 1109–1118, Mar. 2013.
- [10] B. A. P. Nel, A. K. Skrivervik, and M. Gustafsson, "Q-factor bounds for microstrip patch antennas," *IEEE Trans. Antennas Propag.*, vol. 71, no. 4, pp. 3430–3440, Apr. 2023.
- [11] D. Tayli and M. Gustafsson, "Physical bounds for antennas above a ground plane," *IEEE Antennas Wireless Propag. Lett.*, vol. 15, pp. 1281–1284, 2016.

- [12] A. K. Skrivervik, J.-F. Zürcher, O. Staub, and J. R. Mosig, "PCS antenna design: The challenge of miniaturization," *IEEE Antennas Propag. Mag.*, vol. 43, no. 4, pp. 12–27, Aug. 2001.
- [13] K. Fujimoto, A. Henderson, K. Hirasawa, and J. R. James, *Small Antennas* (Antenna Series). Letchworth, U.K.: Research Studies Press, 1988.
- [14] K.-F. Lee and K.-F. Tong, "Microstrip patch antennas—Basic characteristics and some recent advances," *Proc. IEEE*, vol. 100, no. 7, pp. 2169–2180, Jul. 2012.
- [15] Z. Shao and Y. Zhang, "A single-layer miniaturized patch antenna based on coupled microstrips," *IEEE Antennas Wireless Propag. Lett.*, vol. 20, no. 5, pp. 823–827, May 2021.
- [16] H. Mosallaei and K. Sarabandi, "Antenna miniaturization and bandwidth enhancement using a reactive impedance substrate," *IEEE Trans. Antennas Propag.*, vol. 52, no. 9, pp. 2403–2414, Sep. 2004.
- [17] J. R. James, P. S. Hall, and C. Wood, *Microstrip Antenna: Theory and Design*. London, U.K.: Peregrinus on Behalf of the Institution of Electrical Engineers, 1981.
- [18] J. R. Mosig and F. E. Gardiol, "A dynamical radiation model for microstrip structures," in *Advances in Electronics and Electron Physics*, vol. 59, P. W. Hawkes, Ed. New York, NY, USA: Academic, 1982, pp. 139–237.
- [19] R. F. Harrington, *Field Computation by Moment Methods*. New York, NY, USA: Macmillan, 1968.
- [20] M. Gustafsson and M. Capek, "Maximum gain, effective area, and directivity," *IEEE Trans. Antennas Propag.*, vol. 67, no. 8, pp. 5282–5293, Aug. 2019.
- [21] S. P. Boyd and L. Vandenberghe, *Convex Optimization*. Cambridge, U.K.: Cambridge Univ. Press, 2004.
- [22] A. Beck and Y. C. Eldar, "Strong duality in nonconvex quadratic optimization with two quadratic constraints," *SIAM J. Optim.*, vol. 17, no. 3, pp. 844–860, Jan. 2006.
- [23] E. F. Knott, J. F. Shaeffer, and M. T. Tuley, *Radar Cross Section*. vol. 5601 N. Hawthorne Way, Raleigh, NC, USA: SciTech, 2004.
- [24] Y. Su, M. Pellaton, C. Affolderbach, G. Milet, and A. K. Skrivervik, "Mode suppression and homogeneous field bandwidth enhancement of a tuning-free micro-loop-gap resonator using FR4 for chip-scale Rubidium clock," *IEEE Trans. Microw. Theory Techn.*, vol. 72, no. 6, pp. 3711–3721, Jun. 2024.
- [25] J. R. Mosig, R. C. Hall, and F. E. Gardiol, "Numerical analysis of microstrip patch antennas," in *Handbook Microstrip Antennas*, J. R. James and P. S. Hall, Eds. London, U.K.: Peregrinus, 1989, pp. 391–453.
- [26] J. R. Mosig, "Closed formula for the static three-dimensional green function in microstrip structures," *Electron. Lett.*, vol. 14, no. 17, pp. 544–546, Aug. 1978.
- [27] B. A. P. Nel, A. K. Skrivervik, and M. Gustafsson, "Stored energies and Q-factor expressed in material derivatives," *IEEE Antennas Wireless Propag. Lett.*, vol. 23, pp. 19–23, 2024.
- [28] A. D. Yaghjian and S. R. Best, "Impedance, bandwidth, and Q of antennas," *IEEE Trans. Antennas Propag.*, vol. 53, no. 4, pp. 1298–1324, Apr. 2005.
- [29] E. Newman, P. Bohley, and C. Walter, "Two methods for the measurement of antenna efficiency," *IEEE Trans. Antennas Propag.*, vol. AP-23, no. 4, pp. 457–461, Jul. 1975.
- [30] J. M. Jin, *Theory and Computation of Electromagnetic Fields*. Hoboken, NJ, USA: Wiley, 2011.
- [31] R. Harrington and J. Mautz, "Theory of characteristic modes for conducting bodies," *IEEE Trans. Antennas Propag.*, vol. AP-19, no. 5, pp. 622–628, Sep. 1971.



Ben A. P. Nel received the bachelor's degree in electrical and electronic engineering and the master's degree (cum laude) in electronic engineering from Stellenbosch University, Stellenbosch, South Africa, in 2016 and 2019, respectively. He is currently pursuing the Ph.D. degree with the Department of Electrical and Information Technology, Lund University, Lund, Sweden.

His primary research interests include computational electromagnetics.

Mr. Nel was awarded first place in the IEEE Antennas and Propagation Society Student Design Contest in 2023.



Anja K. Skrivervik received the master's and Ph.D. degrees in electrical engineering from the École Polytechnique Fédérale de Lausanne (EPFL), Lausanne, Switzerland, in 1986 and 1992, respectively.

After a stay at the University of Rennes, Rennes, France, as an Invited Research Fellow and two years in the industry, she returned part time to EPFL as an Assistant Professor in 1996, where she was a Professeur Titulaire and the Head of the Microwave and Antenna Group. She was the Director of the EE Section from 1996 to 2000. She is currently the Director of the EE Doctoral School at EPFL. She is also a Visiting Professor at the University of Lund, Lund, Sweden. Her teaching activities include courses on microwaves and antennas, and she teaches at bachelor's, master's, and Ph.D. levels. She is author or co-author of more than 200 peer reviewed scientific publications. Her research interests include electrically small antennas, antennas in biological media, periodic structures, reflect- and transmit-arrays, and numerical techniques for electromagnetics.

Dr. Skrivervik is a Board Member of the European School on Antennas and is frequently requested to review research programs and centers in Europe. She was a member of the Board of Directors of the European Association on Antennas and Propagation (EurAAP) from 2017 to 2022. She received the Latsis Award. She is very active in European collaboration and European projects. She has been the General Chair of the Loughborough Antenna and Propagation Conference in 2015, the Vice-Chair and Technical Program Committee-Chair of the EuCAP 2016 Conference, and the Financial Chair of EuCAP 2017 to EuCAP 2022.



Mats Gustafsson (Senior Member, IEEE) received the M.Sc. degree in engineering physics and the Ph.D. degree in electromagnetic theory from Lund University, Lund, Sweden, in 1994 and 2000, respectively.

He was appointed as a Docent in 2005 and a Professor of electromagnetic theory in 2011, at Lund University. He co-founded the company Phase Holographic Imaging AB, Lund, in 2004. He has written more over 100 peer reviewed journal articles and more over 100 conference papers. His research interests include scattering and antenna theory and inverse scattering and imaging.

Prof. Gustafsson received the IEEE Schelkunoff Transactions Prize Paper Award in 2010, the IEEE Uslenghi Letters Prize Paper Award in 2019, and the Best Paper Awards at EuCAP 2007 and 2013. He served as an IEEE AP-S Distinguished Lecturer from 2013 to 2015.